

Contribution of charge-transfer processes to ion-induced electron emission

M. Rösler*

Departamento de Física de Materiales, Facultad de Química, UPV/EHU, Apartado 1072, 20080 San Sebastián, Spain

F. J. García de Abajo

Departamento de Ciencias de la Computación e Inteligencia Artificial, Facultad de Informática, UPV/EHU, Apartado 649, 20080 San Sebastián, Spain

(Received 3 June 1996)

Charge changing events of ions moving inside metals are shown to contribute significantly to electron emission in the intermediate velocity regime via electrons coming from projectile ionization. Inclusion of equilibrium charge state fractions, together with two-electron Auger processes and resonant-coherent electron loss from the projectile, results in reasonable agreement with previous calculations for frozen protons, though a significant part of the emission is now interpreted in terms of charge exchange. The quantal character of the surface barrier transmission is shown to play an important role. The theory compares well with experimental observations for H projectiles. [S0163-1829(96)07347-X]

I. INTRODUCTION

Ion-induced electron emission constitutes a powerful technique of material analysis. Realistic models of this phenomenon need to incorporate descriptions of electron excitation, transport, and surface barrier crossing.¹

There are different sources of ion-induced electron excitation, namely, direct excitation of target electrons (both conduction band and inner-shell electrons),² plasmon excitation, with the subsequent plasmon decay in which an electron absorbs the plasmon energy,³ target Auger electrons, resulting from the filling of target inner shells previously ionized by the projectile, and electron loss from the ion (ionization).^{4,5}

The projectile can be ionized or neutralized by interaction with the target. Auger and resonant-coherent capture and loss, together with capture from inner shells, seem to be the most relevant processes in this respect.^{4,6,7}

Auger electron loss from the ion involves the simultaneous excitation of a target electron, so that both this electron and the one lost from the ion may contribute to the cascade of electron-hole ($e-h$) pairs accompanying the ion and can eventually escape the solid, increasing in this way the electron emission yield.

Resonant-coherent loss is connected to the periodic perturbation that the solid crystal lattice exerts on the projectile electron.⁷ It takes place when the electron absorbs (in the rest frame of the projectile) an energy equal to one of the harmonics of this potential, being promoted to the continuum. Notice that this mechanism depends on the relative orientation of the ion beam with respect to the target.

Capture and loss have been shown to contribute significantly to the stopping of ions at intermediate velocities^{8,9} (e.g., H^+ at $v \sim 1-2$ a.u.), not only because charge-transfer processes themselves involve energy transfers to the ion, but also as a result of the strong dependence of stopping power on the charge state, since these processes determine the charge state fractions at equilibrium.

Accordingly, capture and loss are expected to play an important role in electron emission at intermediate velocities.

A first attempt to incorporate these processes has already been made by Smidts *et al.*,⁵ assuming that all electrons lost by the ion travel initially with the same velocity as the ion. The motivation of the present work is to give a full description of the charge-transfer processes and their role in the emission properties.

The target will be taken to be a metal whose conduction-band electrons will be described within the free-electron gas model. The interaction between projectile and target will be separated into the dynamic response, which produces Auger processes, and the static crystal potential, responsible for resonant-coherent processes.

Atomic units (a.u.) will be used throughout this work, unless it is stated otherwise.

II. AUGER AND RESONANT-COHERENT ELECTRON LOSS

Let us consider an ion moving inside a solid with velocity \mathbf{v} , carrying a bound electron in state $|0\rangle$ of energy ϵ_0 . The interaction of the electron with the medium produces density fluctuations in the latter, which result in the emergence of an induced potential described here in terms of the dielectric function $\epsilon(q, \omega)$. Due to this perturbation, the bound electron can suffer transitions to excited states of the ion, or even to unoccupied states of the solid valence band, leading to the so-called Auger electron loss processes.^{4,7}

Using many-body techniques, the probability that the bound electron is excited to state $|\mathbf{k}\rangle$ of momentum \mathbf{k} relative to the ion is found to be, within first-order perturbation theory,^{4,6}

$$\begin{aligned} \frac{dP^{\text{Auger}}}{d\mathbf{k}} &= \frac{2}{(2\pi)^3} \theta(|\mathbf{k} + \mathbf{v}| - k_F) \int_0^\infty d\omega \int \frac{d\mathbf{q}}{(2\pi)^3} \frac{4\pi}{q^2} \\ &\times |\langle \mathbf{k} | e^{-i\mathbf{q} \cdot \mathbf{r}} | 0 \rangle|^2 \text{Im} \left\{ \frac{-1}{\epsilon(q, \omega)} \right\} \\ &\times \delta(\mathbf{q} \cdot \mathbf{v} + \epsilon_0 - E - \omega), \end{aligned} \quad (1)$$

where \mathbf{q} and ω represent the momentum and energy transferred to the solid, respectively, $E = k^2/2$ is the electron en-

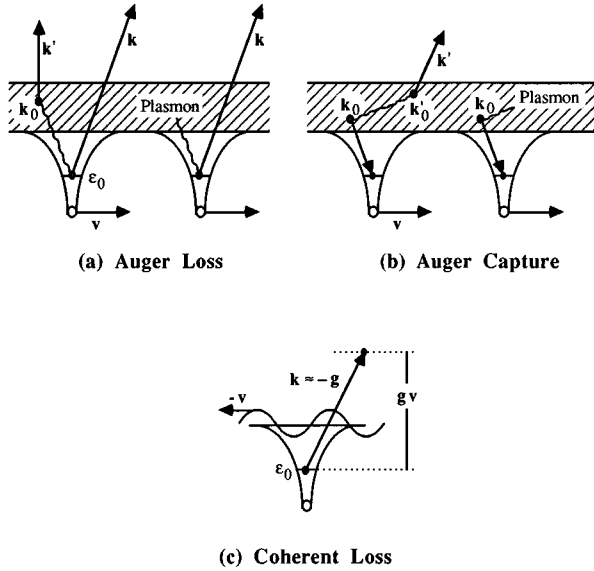


FIG. 1. Schematic representation of (a),(b) Auger and (c) resonant-coherent electron loss processes. (a) Auger electron loss: an electron is promoted from the projectile to the conduction band (dashed region), while an e - h pair (left) or a plasmon (right) is created in the medium. (b) Auger capture: a target electron is trapped by the projectile, while a plasmon or another target electron absorbs the energy released in the process. (c) Resonant-coherent loss: the projectile electron is perturbed by the periodic crystal lattice potential of the target, so that it is promoted to the conduction band, the transition energy corresponding to one of the harmonics of the crystal potential. Resonant-coherent capture can occur in a similar way (see Ref. 7).

ergy, and k_F is the Fermi momentum.

Conduction-band electrons will be described by plane waves orthogonalized to the bound state $|0\rangle$, which will be approximated by a $1s$ wave function $\sqrt{a^3/\pi}e^{-ar}$. The values of ϵ_0 and a , taken from Guinea and Flores,¹⁰ depend on the electron gas density and the projectile velocity. The random-phase approximation (RPA) dielectric function¹¹ will be used in the actual calculations, together with the Mermin prescription¹² in order to introduce finite damping effects (1.35 eV in Al).

Figure 1(a) represents this process schematically. The energy ω released to the medium is converted in either e - h pairs (left) or plasmon excitations (right). The latter can decay via interband transitions, exciting further e - h pairs.¹ This is illustrated in Fig. 2, in which the velocity v_1 is chosen to be large enough to permit the creation of both plasmons and e - h pairs during Auger electron loss, whereas only e - h pairs can be created when the ion moves with the smaller velocity v_2 .

Figure 3 shows the momentum distribution of electrons excited from H projectiles via Auger electron loss (continuous curves), according to Eq. (1) for different ion velocities (see insets). The excitation probability decreases very rapidly with electron energy, and increases with ion velocity within the velocity range under consideration. However, if the ion velocity is large, the ion charge state will be bare protons, which cannot suffer Auger loss. The contribution of e - h pair creation [see Fig. 1(a), left], calculated from Eq. (1) by re-

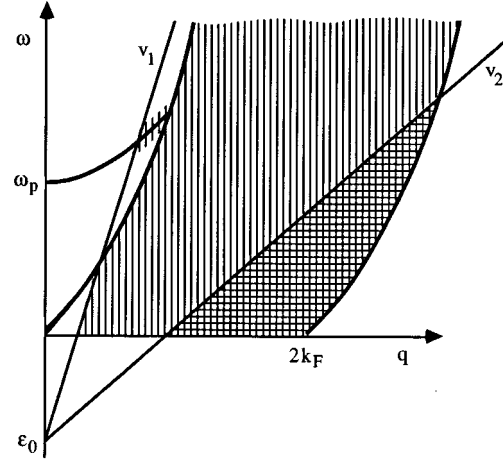


FIG. 2. Representation of the excitations of momentum q and energy $\omega > 0$ that can be created in the solid during Auger electron loss from an atomic level of energy ϵ_0 [see Fig. 1(a)] for two different ion velocities, $v_1 > v_2$. The slope of the inclined straight lines coincides with the ion velocity. The affordable excitations lie on the left-hand side of those lines. Notice that v_1 has been chosen to be large enough to permit the creation of plasmons.

stricting the integral over (q, ω) to the e - h pair region (see Fig. 2), has been represented by dashed curves. This contribution gives nearly the total excitation probability, except for large velocities ($v = 2.2$ a.u. in Fig. 3). This can be understood in terms of the construction shown in Fig. 2. In all cases, plasmon excitation represents a minor contribution, so that the eventual electron emission coming from the deexcitation of these plasmons will be neglected.

Thus, e - h pair creation dominates the Auger loss process in this range of velocities. Using the Fermi golden rule, the probability of creating an electron of momentum \mathbf{k}' relative to the ion (the electron of the e - h pair shown in Fig. 1, left) from the metal Fermi sea during Auger electron loss reduces to

$$\begin{aligned} \frac{dP^{\text{AL}}}{d\mathbf{k}'} &= \frac{2}{(2\pi)^8} \theta(|\mathbf{k}' + \mathbf{v}| - k_F) \\ &\times \int d\mathbf{k} \int d\mathbf{k}_0 \theta(|\mathbf{k} + \mathbf{v}| - k_F) \theta(k_F - |\mathbf{k}_0 + \mathbf{v}|) \\ &\times \left| \langle \mathbf{k} | e^{-i\mathbf{q} \cdot \mathbf{r}} | 0 \rangle \right|^2 \left| \frac{4\pi}{q^2 \epsilon(q, \omega)} \right|^2 \\ &\times \delta\left(\frac{k^2 + k'^2 - k_0^2}{2} - \epsilon_0 \right), \end{aligned} \quad (2)$$

where $\omega = \mathbf{q} \cdot \mathbf{v} + \epsilon_0 - k^2/2$ and $\mathbf{q} = \mathbf{k}' - \mathbf{k}_0$. Equation (2) represents a minor contribution to electron emission, since energy conservation implies that $\epsilon_0 - k^2/2 = k'^2/2 - k_0^2/2$, resulting in electrons of momentum \mathbf{k} moving with velocity close to that of the ion and electrons of momentum \mathbf{k}' near the Fermi level, respectively. The former are already described by Eq. (1), whereas the latter can hardly escape the solid.

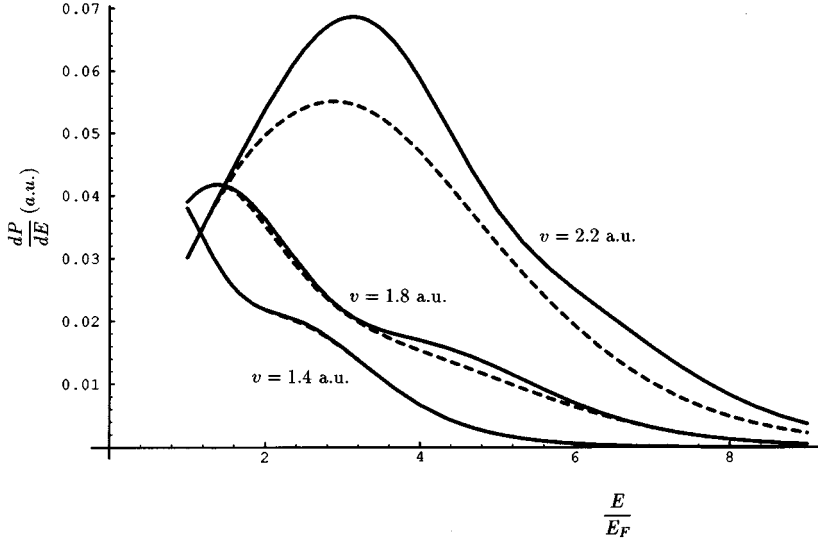


FIG. 3. Energy distribution (in the laboratory frame) of Auger electrons lost from H moving inside aluminum, calculated from Eq. (1) after integrating over the angle $\Omega_{\mathbf{k}}$ (continuous curve), for different ion velocities (see insets). The dashed curves represent the contribution of e - h pair creation [see Fig. 1(a), left].

Accordingly, Auger capture can give rise to the creation of e - h pairs [see Fig. 1(b)]. For electrons originating in Auger neutralization, one finds

$$\begin{aligned} \frac{dP^{AC}}{d\mathbf{k}'} &= \frac{2}{(2\pi)^8} \theta(|\mathbf{k}' + \mathbf{v}| - k_F) \\ &\times \int d\mathbf{k}_0 \int d\mathbf{k}'_0 \theta(k_F - |\mathbf{k}_0 + \mathbf{v}|) \theta(k_F - |\mathbf{k}'_0 + \mathbf{v}|) \\ &\times |\langle \mathbf{k}_0 | e^{i\mathbf{q} \cdot \mathbf{r}} | 0 \rangle|^2 \left| \frac{4\pi}{q^2 \epsilon(q, \omega)} \right|^2 \\ &\times \delta\left(\frac{k_0^2 + k_0'^2 - k'^2}{2} - \epsilon_0\right), \end{aligned}$$

where $\omega = \mathbf{q} \cdot \mathbf{v} - \epsilon_0 + k_0^2/2$ and $\mathbf{q} = \mathbf{k}' - \mathbf{k}'_0$.

The interaction of the projectile with the static crystal potential produces resonant-coherent capture and loss [see Fig. 1(c)]. These can be regarded as elastic processes in the laboratory frame, where the target acts like a source of momentum, in a way similar to what happens in low-energy electron diffraction. The contribution to electron emission coming from those electrons ejected from the projectile via this mechanism will be also accounted for in this work. The differential probability of exciting the bound electron to free state $|\mathbf{k}\rangle$ of momentum \mathbf{k} with respect to the projectile reads, within first-order perturbation theory,¹³

$$\begin{aligned} \frac{dP^{CL}}{d\mathbf{k}} &= \frac{1}{16\pi^3} \theta(|\mathbf{k} + \mathbf{v}| - k_F) \\ &\times \sum_{\mathbf{g}} \int d\Omega_{\mathbf{g}} |V_{\mathbf{g}}^C|^2 |\langle \mathbf{k} | e^{-i\mathbf{g} \cdot \mathbf{r}} | 0 \rangle|^2 \delta\left(\frac{k^2}{2} - \epsilon_0 - \mathbf{g} \cdot \mathbf{v}\right), \end{aligned} \quad (3)$$

where the sum is extended over reciprocal lattice vectors \mathbf{g} , and $V_{\mathbf{g}}^C$ is the corresponding Fourier component of the crystal potential. Equation (3) incorporates the average over different orientations of the target (integral over solid angle $\Omega_{\mathbf{g}}$, appropriate for random orientation of the ion trajectory

or polycrystalline samples. Oriented crystals lead to different angular distribution of excited electrons.¹⁴

The crystal potential will be constructed as a sum of pair potentials using the Ziegler, Biersack, and Littmark (ZBL) approximation.¹⁵ Figure 4 shows the momentum distribution of excited electrons, calculated using Eq. (3) for H and H⁻ projectiles moving in Al. The different maxima can be understood in terms of momentum and energy conservation, expressed in Eq. (3) by the matrix element and the δ function, respectively. Momentum conservation requires $\mathbf{k} \approx -\mathbf{g}$ — otherwise the form factor becomes negligible. Then, energy conservation leads to

$$\mathbf{k} \cdot \mathbf{v} \approx \epsilon_0 - \frac{k^2}{2}. \quad (4)$$

In particular, the symbols \times , $+$, Δ , and \circ in Fig. 4 refer to vectors \mathbf{k} obtained from Eq. (4) for reciprocal lattice vectors $\langle 1,1,1 \rangle$, $\langle 2,0,0 \rangle$, $\langle 2,2,0 \rangle$, and $\langle 1,1,3 \rangle$, respectively (notice that Al is an fcc crystal for which $V_{\mathbf{g}}^C$ vanishes unless $\mathbf{g} = [i, j, k]$ is such that i , j , and k are either all even or all odd numbers).

III. TRANSPORT MODEL

A. General considerations

Different methods have been proposed to describe particle-induced electron emission.^{16–19,1} Besides the description based on principles similar to sputtering theory,^{16,17} some authors have performed calculations of the emission features within Monte Carlo schemes, using simplified expressions for the different basic scattering quantities.^{18,19} The transport equation formalism^{1,20,18} has been chosen in the present work, including a detailed microscopic description of the scattering quantities.^{1,20}

In addition to the processes of electron excitation discussed in the previous section, there are different competing mechanisms responsible for the emission. The scattering processes within the target are the same in all cases, with independence of the source of excited electrons (either the target or the projectile). Within the framework of transport theory,

the basic relation that allows us to determine the density of excited electrons per unit electron energy E around the solid angle Ω , that is, $N(E, \Omega)$, may be written as¹

$$\frac{v_e(E)}{l(E)} N(E, \Omega) = S(\mathbf{v}; E, \Omega) + \int_E^\infty dE' \times \int d\Omega' W(E, \Omega; E', \Omega') N(E', \Omega'), \quad (5)$$

where $v_e(E)$ is the velocity and $l(E)$ the total mean free path (mfp) of the electron. The left-hand side of this equation represents the number of electrons that are scattered out of state $\mathbf{k}(E, \Omega)$. The second term on the right-hand side is the number of electrons entering state \mathbf{k} by collisions with the target. This number is expressed in terms of the transition function $W(E, \Omega; E', \Omega')$. The amount of electrons created in state \mathbf{k} by the impinging particle is described by the excitation function $S(\mathbf{v}; E, \Omega)$.

Both the mfp and the transition function reflect target properties. These quantities are determined by elastic and inelastic scattering processes. It should be noted that, due to the distinct anisotropy of the excitation of single conduction electrons¹ as well as projectile electrons, elastic scattering is of fundamental importance when calculating the emission features.

Elastic cross sections can be obtained following standard partial wave analysis techniques. The phase shifts will be determined by using Smrčka's muffin tin potential for Al.²¹ The inelastic scattering of excited electrons will be described neglecting its interaction with core electrons. The inelastic mfp is given by the well-known random-phase-approximation (RPA) result²² (contribution from single conduction electrons and from plasmon excitation).

Different processes contribute to the inelastic part of the transition function, which can be written for electrons^{1,23,20} (arguments will be dropped)

$$W^{\text{inel}} = W_e + W_e^s + W_p + W_p^s. \quad (6)$$

The first two terms on the right-hand side describe single-electron scattering, including the rates of transition and excitation, W_e and W_e^s , respectively.²³ These quantities are responsible for the development of the cascade maximum in the energy spectra of emitted electrons at low energies. The other two terms in this equation are related to plasmon processes. W_p describes the change in the state of excited electrons when they create plasmons. Finally, W_p^s describes the excitation of target electrons by the decay of those plasmons.

The first three terms in the sum of Eq. (6) can be described within the free-electron gas model in the RPA. However, since the most important contribution to plasmon damping originates in interband processes in simple metals,²⁴ the evaluation of W_p^s requires one to go beyond that model.³ Explicit expressions for all these contributions are given in previous works.^{1,20}

The escape process will be described by the simple model of a planar-surface square barrier potential. The barrier height W is given in metals by the sum of the Fermi energy and the work function: $W = E_F + \Phi$. Apart from a few exceptions,²⁵ the transmission of excited electrons through the surface has been mainly described classically in the past.

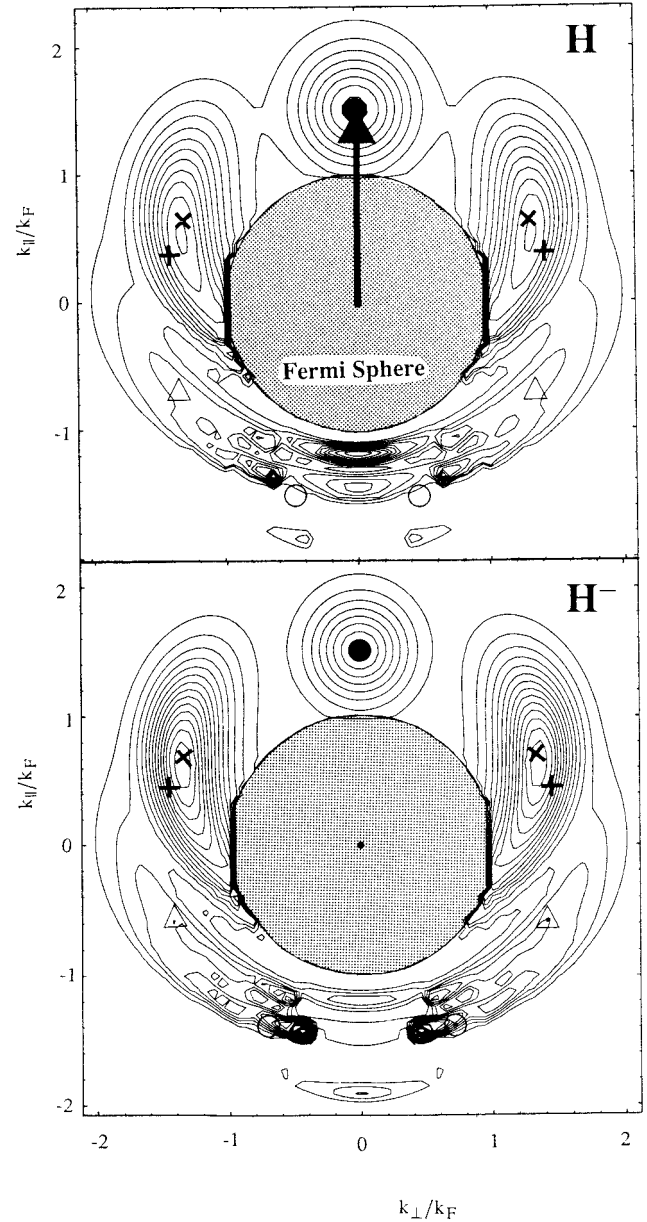


FIG. 4. Contour plots representing the momentum distribution (in the laboratory frame) of electrons excited to the continuum via coherent electron loss from H (upper figure) and H^- (lower figure) moving in aluminum with velocity $v = 1.4$ a.u. The projectile velocity has been represented by a vertical arrow for H. k_{\parallel} and k_{\perp} refer to momentum components parallel and perpendicular to the velocity, respectively. The symbols \times , $+$, Δ , and \circ refer the maxima in the distribution related to different harmonics, as explained in the text.

This means that the transmission probability of excited electrons, $T(E, \cos\alpha)$, which depends in general on the energy and the direction of propagation of the electron (α is the angle between the wave vector \mathbf{k} and the surface normal), is taken to be 1 for electrons moving towards the surface within the so-called escape cone and vanishes otherwise. The escape cone angle α_c is defined by $\cos\alpha_c = \sqrt{W/E}$. A simple quantum-mechanical calculation for a square barrier leads to²⁶

$$T(E, \cos \alpha) = \frac{4\sqrt{1 - W/(E \cos^2 \alpha)}}{[1 + \sqrt{1 - W/(E \cos^2 \alpha)}]^2}, \quad (7)$$

which lies distinctly below 1 at low electron energies. Therefore, the quantum character of the barrier should be included in a calculation of the emission properties.

B. Special aspects concerning the excitation functions

Excitation of inner shell electrons of target atoms is of minor importance within the ion velocity range under consideration (less than 6%). Therefore, the dominant mechanisms are direct Coulomb excitation of valence electrons and decay of plasmons generated by the projectile. The corresponding excitation functions will be denoted S_e and S_p , respectively. Explicit expressions can be found in the literature.^{1,20,3}

The excitation of projectile electrons discussed in Sec. II will be shown to be important as well. The excitation probabilities for Auger and resonant-coherent processes [Eqs. (1) and (3), respectively] permit one to obtain the excitation functions, which read, written in the variables used in Eq. (5),

$$S_X^{\text{Auger}}(\mathbf{v}; E, \cos \theta) = \frac{2\pi v_e}{v} \frac{dP^{\text{Auger}}}{d\mathbf{k}},$$

$$S_X^{\text{CL}}(\mathbf{v}; E, \cos \theta) = \frac{2\pi v_e}{v} \frac{dP^{\text{CL}}}{d\mathbf{k}},$$

where X refers to the ion charge state, H or H^- , respectively, and θ is the angle between \mathbf{k} and \mathbf{v} .

The solution of Eq. (5) in the angular coordinate can be obtained by expansion in terms of Legendre polynomials. This method works very well also in cases of anisotropic excitation functions. Figure 5 shows the angular dependence of the excitation of projectile electrons by Auger loss. These electrons are excited preferentially in the forward direction. It should be noted that the angular distribution of excited electrons is not well represented by a small number of terms in this case. Nevertheless, reliable results can be obtained with sufficient accuracy with a restricted number of terms, due to the relevant role played by the strong elastic scattering, especially at low electron energies. The original anisotropy of the excitation is removed to a large extent by these scattering processes.

C. Measurable quantities

The measurable quantities in the electron emission phenomena are the energy-angular distributions of emitted electrons and the electron yield γ . They can be determined by solving Boltzmann transport equation (5) for the different excitation mechanisms, eventually including the escape conditions at the surface.

The electron yield derived from Eq. (5) may be written as (see Ref. 1)

$$\gamma = 2\pi \sum_{l=0}^{\infty} \int_W^{\infty} dE v_e(E) A_l(E) N_l(E),$$

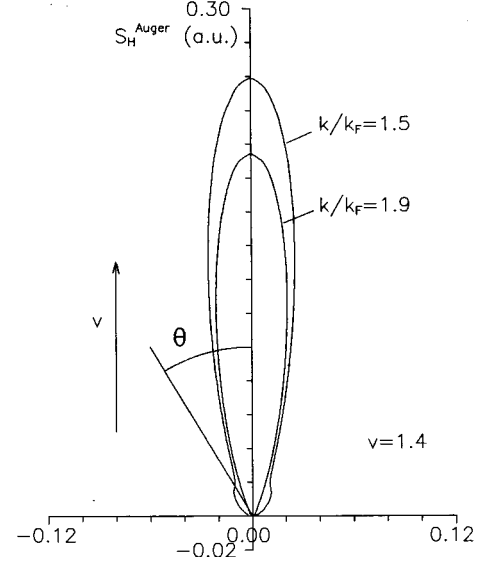


FIG. 5. Angular distribution of electrons excited by Auger electron loss from H for different excitation energies. The momentum of excited electrons is given in units of the Fermi momentum: $k/k_F = 1.5$ and 1.9 . The distance to the origin corresponds to the value of S_H^{Auger} in a.u., θ denotes the excitation angle, and v is the ion velocity.

where N_l is the l coefficient of N in a Legendre polynomial expansion. The factor $A_l(E)$ reflects the special choice of the escape model by inclusion of the transmission probability $T(E, \cos \alpha)$:

$$A_l(E) = \int_{\sqrt{W/E}}^1 x dx P_l(x) T(E, x),$$

where P_l is the Legendre polynomial of order l .

Previous theories of ion-induced kinetic electron emission^{1,18} are based on the assumption of frozen charge state of the impinging ion during its passage through the target region defined by the maximum escape depth of excited electrons. Now, when the contribution to the emission related to the different charge states of the projectile is taken into account, the total electron yield is given by summing the contribution of each species, weighted with the respective charge state fraction. For protons, one obtains

$$\begin{aligned} \gamma^{\text{total}} = & (\Phi^+ + \Phi^-) \gamma^0 + \Phi^0 (\gamma_H^{\text{Auger}} + \gamma_H^{\text{CL}}) \\ & + 2\Phi^- (\gamma_{H^-}^{\text{Auger}} + \gamma_{H^-}^{\text{CL}}), \end{aligned} \quad (8)$$

where γ^0 represents the yield obtained for frozen-charge-state bare protons, that is, when only the direct excitation of single conduction electrons S_e and the excitation by plasmon decay S_p are considered. γ_X^{Auger} and γ_X^{CL} stand for the contribution of Auger and resonant-coherent processes to the yield, respectively, both for neutrals ($X=H$) and negative ions ($X=H^-$). A factor of 2 has been included in the last term of Eq. (8) to reflect the fact that H^- carries two electrons.

IV. RESULTS AND DISCUSSION

The results obtained for ion-induced kinetic electron emission from the theory described above, including charge-

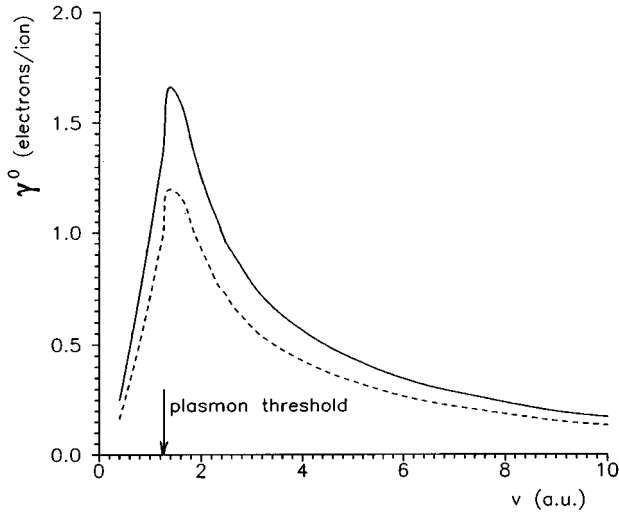


FIG. 6. Projectile velocity dependence of the backward electron yield γ^0 produced by bare protons for different descriptions of the surface barrier transmission: classical (solid curve) and quantal [dashed curve; see Eq. (7)].

transfer processes at intermediate ion velocities, will be discussed in this section.

In Sec. III C, a quantum-mechanical description of the transmission of excited electrons through the surface [Eq. (7)] was incorporated. Figure 6 is intended to demonstrate the important role played by this transmission description. It shows the velocity dependence of the backward electron yield for bare protons (i.e., without considering charge exchange) using classical (solid curve) and quantal (dashed curve) transmission factors. Notice that the quantum-mechanical description leads to a considerable reduction in the number of emitted electrons, so that it will be employed in what follows.

The solution of Boltzmann equation (5) leads to the same qualitative behavior of the energy spectra of emitted electrons at low energies for all the mechanisms of electron excitations described above, with the single exception of the excitation by the decay of plasmons generated by the impinging ion. The threshold of ion velocity for creating plasmons in Al (≈ 1.27 a.u.) has been marked in Fig. 6. In this case, the strong decrease in the excitation rate at electron energies above $E_F + \omega_p$, where ω_p is the plasmon energy, is not influenced by the transport process. Therefore, this behavior of the excitation function is directly reflected in the energy spectrum of emitted electrons. This so-called plasmon shoulder is clearly observed for Al in the experiments.²⁷

The different mechanisms of excitation of projectile electrons lead to energy distributions of excited electrons that are smoothly decreasing functions of the excitation energy (see Fig. 3). Therefore, the solution of the Boltzmann equation for these excitation processes does not produce unusual features in the corresponding energy distribution of emerging electrons. We will restrict ourselves exclusively to the discussion of the backward electron yield produced by proton impact on Al from now on.

The main result of the present calculation is presented in Fig. 7. For completeness, the upper part of the figure shows the equilibrium charge state fractions of different species (H,

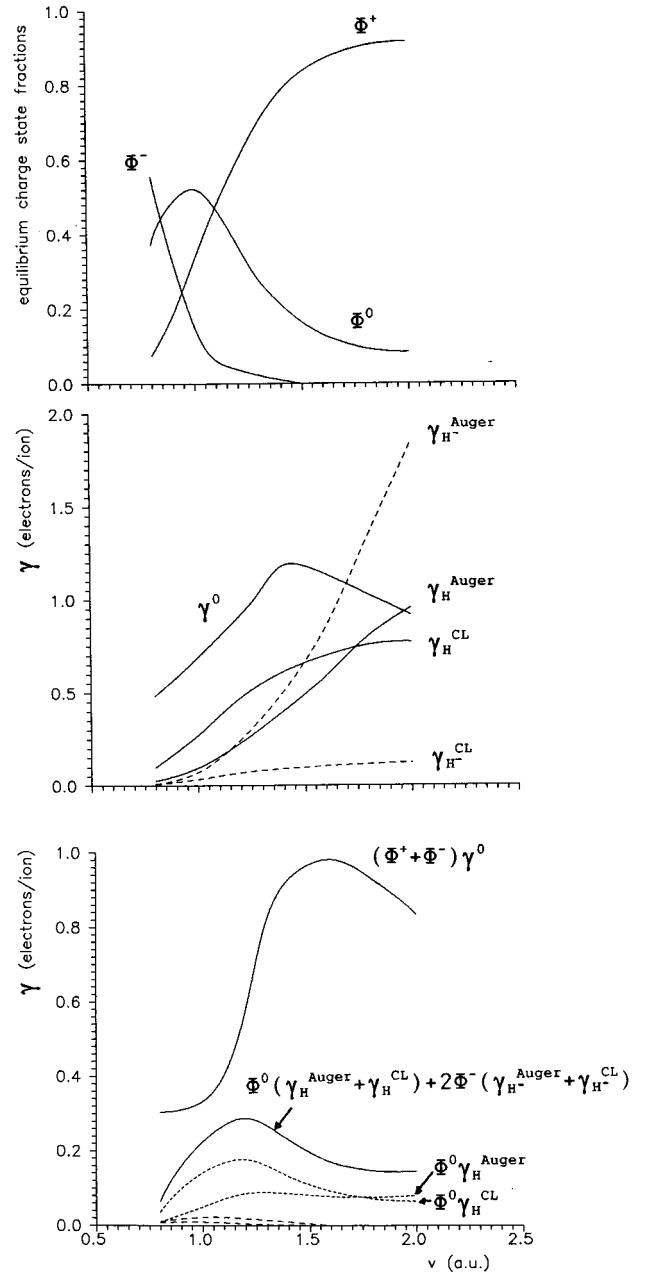


FIG. 7. (a) Upper part. Equilibrium charge state fractions as a function of the ion velocity for H moving in aluminum: neutral fraction (Φ^0), H^- fraction (Φ^-), and bare proton fraction (Φ^+). (b) Intermediate part. Backward electron yield related to different excitation mechanisms: target electrons excited by H^+ projectiles, γ^0 ; projectile electrons lost from H via Auger and coherent loss, γ_H^{Auger} and γ_H^{CL} respectively; the same for H^- , $\gamma_{H^-}^{Auger}$ and $\gamma_{H^-}^{CL}$. (c) Lower part. Contribution to the electron yield coming from different processes including the equilibrium charge fractions (from the upper part). The unlabeled long-dashed curves represent the contribution H^- : $2\gamma_{H^-}^{Auger}\Phi^-$ (upper curve) and $2\gamma_{H^-}^{CL}\Phi^-$ (lower curve).

H^- , and H^+), calculated by Peñalba *et al.*⁹ taking into account capture from target inner-shell electrons, as well as Auger and resonant-coherent capture and loss. The intermediate part shows the electron yield calculated from Eq. (5) for the excitation mechanisms discussed in Sec. II, assuming frozen charge states. The actual contribution of different

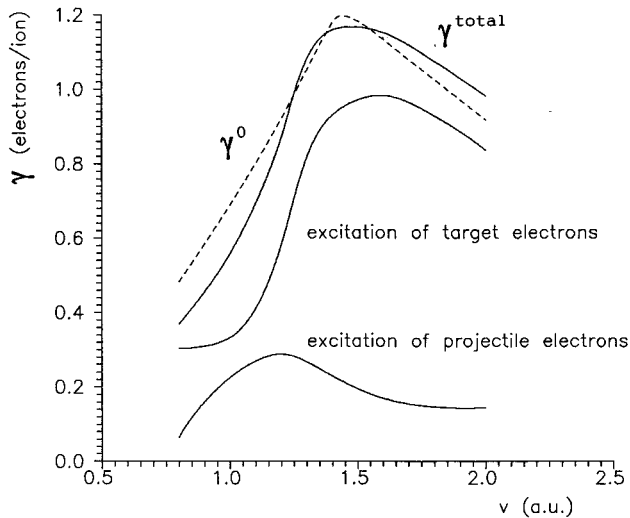


FIG. 8. Total backward electron yield produced by proton bombardment of an aluminum surface under normal incidence, as a function of ion velocity (upper solid line), decomposed in electrons coming from target and projectile. The results obtained by considering frozen-charge-state protons (γ^0) are also included for comparison (dashed line).

charge state fractions to the total electron yield is then obtained by multiplying the data displayed in these sub-figures (lower part).

The contribution of electron loss from neutrals dominates over that of negative ions, as can be observed in Fig. 7 (lower part). The electron yield related to the excitation of target electrons is dominant in the upper end of the ion velocities under consideration. For velocities around 1 a.u. (near the Fermi velocity in Al) both types of excitation (target and projectile electrons) give comparable contributions to the electron yield.

The electron yield calculated by taking into account charge state effects is compared with the yield obtained with the approximation of frozen-charge-state protons in Fig. 8 (solid and broken curves, respectively). Surprisingly, the two calculations lead to nearly the same result for the velocity dependence of the total electron yield. However, the physical origin of the emission (i.e., the underlying microscopic processes) is different in both cases.

Figure 9 offers a comparison of the present calculations with available experimental results for proton impact on polycrystalline Al, obtained by various groups.²⁸⁻³¹ Reasonable agreement between theory and experiment is observed in the region of maximum yield. However, the calculated values of the total yield are below the experimental ones at ion velocities above the maximum and distinctly below at low ion velocities.

Previous calculations have shown that elastic scattering is very important for a proper description of the emission phenomenon. In the excitation of single conduction electrons (S_e), elastic scattering leads to a considerable enhancement of the number of excited electrons that are able to leave the target.³² Auger electrons are strongly peaked in the forward direction, as can be seen in Fig. 5, so that also in this case, elastic scattering produces a dramatic enhancement in the

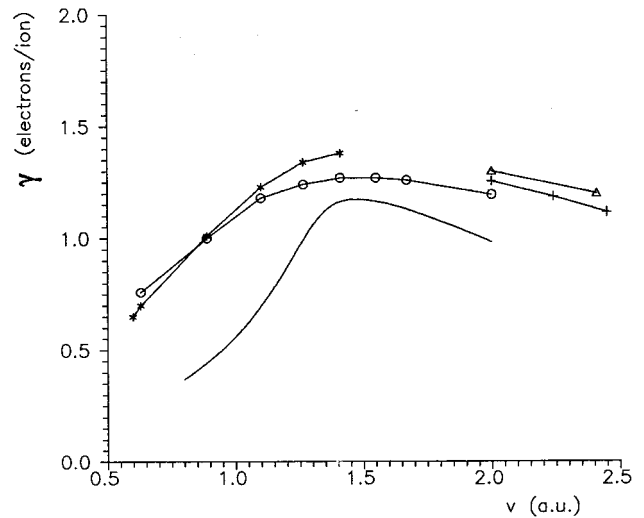


FIG. 9. Comparison of the present theory (solid curve) with available experimental results for the backward yield of electron emission induced by proton bombardment of polycrystalline Al under normal incidence. Experimental data: *, O, Δ, and + are taken from Refs. 1, 29, 30 and 31, respectively.

contribution of this mechanism to the backward yield, as shown in Fig. 10.

V. CONCLUSIONS

Starting from the microscopic description of electron excitation and scattering, and using the transport equation approach, previous calculations of ion-induced electron emission properties based on the assumption of frozen charge states have been extended, taking into account different charge-transfer processes as well as charge state fractions in the projectile beam.

A parameter-free calculation has been performed for proton impact on polycrystalline aluminum using an improved

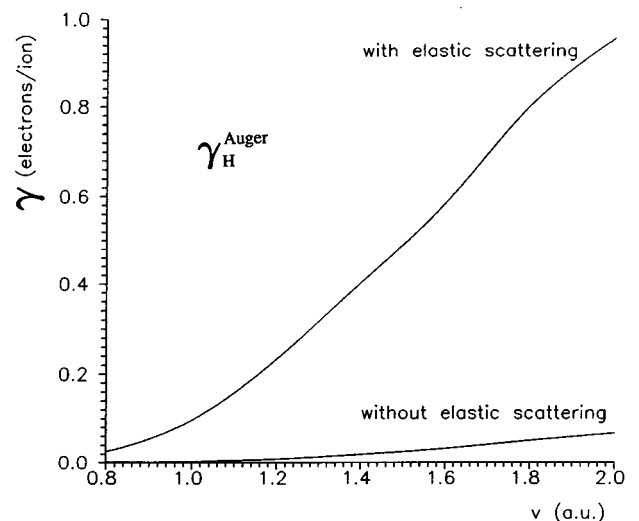


FIG. 10. Contribution of Auger electron loss to the backward electron yield under the same conditions as in Fig. 9, with and without including elastic scattering in the transport process.

quantal description of the escape process. The different contributions to the electron yield coming from the excitation of target and projectile electrons are considered separately. The contribution of projectile electrons is shown to be important for protons moving with velocities in the region of 1 a.u. Excitation of target electrons dominates at larger velocities.

Comparison of the present model with previous theories shows that the total backward electron yield is nearly the same in both cases for protons moving within the range of ion velocities under consideration (see Fig. 8).

Reasonable agreement is obtained between theory and experiment (Fig. 9). However, the calculated values lie distinctly below the experimental result, especially at low velocities. Various effects could partially account for this difference: potential emission provides a small contribution of the order of $0.06e^-/\text{ion}$;³³ nonlinear effects lead to an enhancement of the calculated stopping power of protons moving in metals at low velocities,³⁴ so that a similar trend is

expected to occur in electron emission; the preequilibrium region, expected to become relevant with decreasing ion velocity, is not treated properly in this work.

It should be stressed that elastic scattering plays a fundamental role in the emission, due to the strong anisotropy of the electron excitation function. In particular, Auger electrons lost from the projectiles are preferentially directed towards the bulk of the material (Fig. 5). Elastic scattering deflects them towards the vacuum side, thus increasing the electron yield associated with this excitation process.

ACKNOWLEDGMENTS

Technical support from Juan Pablo Fernández Ramírez is gratefully acknowledged. One of the authors (F.J.G.A.) acknowledges help and support from the Departamento de Educación del Gobierno Vasco and the Basque Country University.

*Permanent address: Institute of Physics, Humboldt University, Invalidenstrasse 110, D-10115 Berlin, Germany.

¹M. Rösler and W. Brauer, in *Particle Induced Electron Emission I* (Springer-Verlag, Berlin, 1991), Vol. 122, pp. 1–65.

²R. H. Ritchie, *Phys. Rev.* **114**, 644 (1959).

³M. S. Chung and T. E. Everhart, *Phys. Rev. B* **15**, 4699 (1977).

⁴F. Guinea, F. Flores, and P. M. Echenique, *Phys. Rev. Lett.* **47**, 604 (1981).

⁵C. Smidts *et al.*, *Nucl. Instrum. Methods B* **67**, 646 (1992).

⁶F. Guinea, F. Flores, and P. M. Echenique, *Phys. Rev. B* **25**, 6109 (1982).

⁷F. Sols and F. Flores, *Phys. Rev. B* **30**, 4878 (1984).

⁸A. Arnau *et al.*, *Phys. Rev. Lett.* **65**, 1024 (1990).

⁹M. Peñalba *et al.*, *Europhys. Lett.* **19**, 45 (1992).

¹⁰F. Guinea and F. Flores, *J. Phys. C* **13**, 4137 (1980).

¹¹J. Lindhard, K. Dan. Vidensk. Selsk. Mat. Fys. Medd. **28**, No. 8 (1954).

¹²N. D. Mermin, *Phys. Rev. B* **1**, 2362 (1970).

¹³P. M. Echenique, F. Flores, and R. H. Ritchie, *Solid State Phys.* **43**, 229 (1990).

¹⁴F. J. García de Abajo, V. H. Ponce, and P. M. Echenique, *Phys. Rev. Lett.* **69**, 2364 (1992); *Phys. Rev. B* **49**, 2832 (1994).

¹⁵J. F. Ziegler, J. P. Biersack, and U. Littmark, in *Proceedings of the International Ion Engineering Congress, ISIAT'83 & IPAT'83*, edited by J. F. Ziegler (Pergamon, New York, 1983), p. 1861.

¹⁶J. Schou, *Phys. Rev. B* **22**, 2141 (1980).

¹⁷J. Schou, *Scanning Microsc.* **2**, 607 (1988).

¹⁸J. Devooght *et al.*, *Particle Induced Electron Emission I* (Springer-Verlag, Berlin, 1991), pp. 67–128.

¹⁹A. Dubus *et al.*, *Phys. Rev. B* **47**, 8056 (1993).

²⁰M. Rösler, *Scanning Microsc.* **8**, 3 (1994).

²¹L. Smrčka and J. Czech, *J. Phys. B* **20**, 291 (1970).

²²J. J. Quinn, *Phys. Rev.* **126**, 1453 (1962).

²³C. J. Tung and R. H. Ritchie, *Phys. Rev. B* **16**, 4302 (1977).

²⁴K. Sturm, *Adv. Phys.* **31**, 1 (1982).

²⁵T. Kaneko, *Surf. Sci.* **237**, 327 (1990).

²⁶E. Merzbacher, *Quantum Mechanics* (Wiley International, New York, 1970).

²⁷D. Hasselkamp, in *Particle Induced Electron Emission II* (Springer-Verlag, Berlin, 1992), Vol. 123, pp. 1–95.

²⁸R. A. Baragiola, E. V. Alonso, and A. Oliva-Florio, *Phys. Rev. B* **20**, 121 (1979).

²⁹B. Svensson and G. Holmen, *J. Appl. Phys.* **52**, 6928 (1981).

³⁰D. Hasselkamp, K. G. Lang, S. Scharmman, and N. Stiller, *Nucl. Instrum. Methods* **180**, 349 (1981).

³¹S. Hippler, Ph.D. thesis, University of Giessen, 1988.

³²M. Rösler, *Nucl. Instrum. Methods B* **78**, 263 (1993).

³³P. Varga and H. Winter, in *Particle Induced Electron Emission II* (Springer-Verlag, Berlin, 1992), Vol. 123, pp. 149–213.

³⁴P. M. Echenique, F. J. García de Abajo, V. H. Ponce, and M. E. Uranga, *Nucl. Instrum. Methods B* **96**, 583 (1995).